

# Self-enrichment in Globular Clusters: the extreme He-rich population of NGC 2808

Di Criscienzo, M.<sup>1</sup>, Ventura<sup>1</sup> P., D’Antona<sup>1</sup> F., Dell’Agli<sup>2,3</sup>, F. & Tailo, M.<sup>4</sup>

<sup>1</sup>*INAF – Osservatorio Astronomico di Roma, Via Frascati 33, 00078, Monte Porzio Catone (RM), Italy*

<sup>2</sup>*Instituto de Astrofísica de Canarias, E-38205 La Laguna, Tenerife, Spain*

<sup>3</sup>*Departamento de Astrofísica, Universidad de La Laguna (ULL), E-38206 La Laguna, Tenerife, Spain*

<sup>4</sup>*Dipartimento di Fisica e Astronomia ‘Galileo Galilei’, Univ. di Padova, Vicolo dell’Osservatorio 3, I-35122 Padova, Italy*

Accepted, Received; in original form

## ABSTRACT

Almost several decades after the discovery of the first multiple populations in galactic globular clusters (GC) the debate on their formation is still extremely current and NGC2808 remains one of the best benchmark to test any scenario for their origin and the evolution. In this work we focus on the chemical composition of stars belonging to the extreme He-rich population populated by stars with the most extreme abundance of Mg, Al, Na, O and Si. We checked whether the most recent measures are consistent with the AGB yields of stars of  $6.5 - 8 M_{\odot}$ . These stars evolve on time scales of the order of 40-60 Myr and eject matter strongly enriched in helium, owing to a deep penetration of the surface convective zone down to regions touched by CNO nucleosynthesis occurring after the core He-burning phase. Since the big unknown of the AGB phase of massive stars is the mass loss, we propose a new approach that takes into account the effects of the radiation pressure on dust particles. We show that this more realistic description is able to reproduce the observed abundances of Mg, Al, Na and Si in these extreme stars. The large spread in the oxygen abundances is explained by invoking deep mixing during the RGB phase. It will be possible to check this work hypothesis as soon as the oxygen measurements of the main sequence stars of NGC2808 will be available.

**Key words:** Stars: abundances – Stars: AGB and post-AGB – Globular Clusters: general – Globular Clusters. individual: NGC 2808

## 1 INTRODUCTION

The recent decades have witnessed a growing interest towards the evolution of Globular Clusters (GC). Results from high resolution spectroscopy, photometry and spectrophotometry, have shown that Galactic GC harbour a variety of stellar populations, differing in their chemical composition. This is at odds with the classic, traditional assumption, that GC are simple stellar populations, composed by coeval and chemically homogeneous stars.

All the GC of the Milky Way so far examined present star-to-star variations, which trace well defined abundance patterns, such as the C-N and O-Na anti-correlations, whose extension varies from cluster to cluster (Gratton et al. 2012). These abundance variations were observed also at the surface of unevolved stars (e.g. Gratton et al. 2001); for these stars, unlike red giants, can be disregarded the effects of any possible ‘in situ’ production mechanism able to reproduce at the same time all the chemical patterns. A plausible interpretation of these observations is that in GC a variety of generations of stars coexist, each characterized

by a different chemical composition. This conclusion is further reinforced by the observations indicating that some GC also exhibit a Mg-Al trend (Kraft et al. 1997; Gratton et al. 2001; Carretta et al. 2009; Mészáros et al. 2015), involving two species, Mg and Al, whose surface abundance remains unchanged during the red giant branch (hereinafter RGB) evolution, even in case of deep mixing.

NGC 2808 has so far played a pivotal role in the ongoing debate regarding the modality with which new generations of stars formed in GC, after the birth of the original population. The great interest towards this cluster is motivated by the complex morphology of the horizontal branch (HB) and the peculiar distribution of stars across the main sequence (MS). The HB has a clumpy structure, with some gaps in the distribution of stars in the colour-magnitude diagram (CMD) (Bedin et al. 2000); the MS exhibits a significant spread in colour, and is split into three discrete sequences (D’Antona et al. 2005; Piotto et al. 2007).

These results indicate the presence of three groups of stars, differing in the helium content,  $Y$ : a) the primordial

arXiv:1807.00859v1 [astro-ph.SR] 2 Jul 2018

population, with  $Y = 0.25$ , which correspond to the stars on the red side of the HB and on the red main sequence; b) the bluest and faintest objects in the HB, the counterparts of the stars populating the blue MS, with  $Y > 0.35$ ; c) the "intermediate" population, with helium  $0.27 < Y < 0.30$  (D'Antona & Caloi 2004; D'Antona et al. 2005; Piotto et al. 2007). Bragaglia et al. (2010) performed a chemical tagging of two stars belonging, respectively, to the He-normal and He-rich main sequences, finding that the blue-MS star shows a huge enhancement of N, a depletion of C, an enhancement of Na and Al, and a small depletion of Mg, with respect to the red MS star. This is exactly what is expected if stars on the blue MS formed from the CNO-processed ejecta produced by an earlier stellar generation.

The recent analysis by Milone et al. (2015), based on HST UV data from the Legacy Survey of Galactic globular Clusters (Piotto et al. 2015), outlined an even more complex stellar population, suggesting that NGC 2808 harbours 5 groups of stars, differing in their chemical composition.

D'Antona et al. (2016), in the context of the scenario based on self-enrichment by massive AGB stars (Ventura et al. 2001; D'Ercole et al. 2008), proposed a temporal sequence for the formation of the various populations in NGC 2808. In particular the stars belong to population E, according to the classification by Milone et al. (2015), formed 40-60 Myr after the formation of the cluster, directly from the ejecta of AGB stars of mass 7-8  $M_{\odot}$ , after the end of SNII that means with no dilution with pristine gas. Because the ejecta of massive AGB stars are enriched in helium, we know from stellar evolution theories that stars born with this chemical composition would populate the blue side of the HB during the core helium burning phase (D'Antona et al. 2002) and would define a blue MS during the core hydrogen burning evolution; this would explain the peculiar distribution of NGC 2808 stars in the CMD.

Assessing the reliability of the framework proposed by the afore mentioned works can be considered as a general test for the AGB self-enrichment scenario itself. NGC 2808 is by far the most complex GC so far investigated: the capability to reproduce all the observations collected so far would be a strong point in favour of any theoretical schematization. The present investigation falls within this context. The recent high-resolution spectroscopy results by Carretta et al. (2018) allow a significant step forward towards this direction. This work, coupled with the results by Carretta (2015), presents data regarding all the light elements, including Mg, Al and Si, whose abundances were not considered in the analysis by D'Ercole et al. (2010) and D'Antona et al. (2016).

In this paper we want to test the scenario proposed by D'Antona et al. (2016) for the star formation history of NGC 2808. We focus on the chemical composition of stars belonging to the population E, to check whether their observed surface abundances are consistent with the AGB yields of stars of  $6.5 - 8 M_{\odot}$  (SAGB).

The paper is structured as follows: in section 2 we present an overview of the self-enrichment scenario by AGB stars, whereas section 3 focuses on the importance of NGC 2808 in the current debate on the formation of multiple population in GC; in section 4 we present the SAGB models, calculated on purpose for this work, with the same chemical composition of the stars belonging to primordial population

of NGC 2808; section 5 presents a comparison between the yields of massive AGB stars with the chemical composition of the NGC 2808 stars in the group E. The conclusions close the paper and are given in section 6.

## 2 SELF-ENRICHMENT BY AGB STARS

According to the AGB scenario for self-enrichment in globular clusters, the formation of new stellar generations began after the epoch of type II SNe explosions, from the ashes of stars of mass  $4 M_{\odot} < M < 8 M_{\odot}$ , belonging to the first generation (FG) (Ventura et al. 2001; D'Ercole et al. 2008). During the AGB phase these objects lose the external mantle, releasing gas processed by hot bottom burning (HBB), which consists into the proton-capture nuclear activity experienced at the base of the external envelope (Renzini & Voli 1981; Blöcker & Schönberner 1991).

The chemical composition of the stars belonging to the newly formed second generation (SG) of the cluster is determined by the complex interplay among the metallicity, the dilution of the AGB gas with pristine matter, the epochs when dilution began and when the formation of the SG was halted by type Ia SN explosions (D'Ercole et al. 2011; Vesperini et al. 2013; D'Antona et al. 2016; D'Ercole et al. 2016).

The interpretation of the observed abundances of SG stars requires the use of dilution curves, calculated by assuming mixing of AGB ejecta with various percentages of pristine matter, with the same chemical composition of FG stars (Ventura & D'Antona 2008, 2009; Ventura et al. 2016; D'Antona et al. 2016; Dell'Agli et al. 2018). This makes the understanding of the observed chemical patterns more complicated, as the results obtained are sensitive to the efficiency of different physical phenomena, primarily HBB, dilution and mass loss.

### 2.1 The signature of SAGB stars in Globular clusters with extreme populations

A robust evaluation of the reliability of any self-enrichment scenario and a straightforward reconstruction of the star formation history of the cluster is possible when part of the SG formed directly from the gas expelled by the polluters. In this particular case the AGB scenario can be tested by comparing the surface abundances of FG stars with the chemical composition of the AGB ejecta. The clusters harbouring this class of stars can be easily identified, because the presence of fully contaminated SG stars is associated to an evident blue tail characterizing the HB morphology (D'Antona et al. 2002; D'Antona & Caloi 2004), determined by the large helium enrichment.

This approach was followed by Di Criscienzo et al. (2011, 2015) and Ventura et al. (2016) to study the formation of multiple populations in NGC 2419 and by Tailo et al. (2015, 2016) to investigate the various stellar groups in  $\omega$  Centauri; these are the other two Galactic clusters, together with NGC2808, which harbour an extreme SG, likely formed without dilution with pristine gas.

In the AGB self-enrichment scenario the formation of stars strongly enriched in helium from gas undiluted with pristine matter can occur within 10-20 Myr since the end of

the epoch of type II SNe explosions, from the winds of stars of initial mass in the range  $7 - 8 M_{\odot}^1$ . These stars evolve on time scales of the order of 40-60 Myr and eject matter strongly enriched in helium, owing to a deep penetration of the surface convective zone down to regions touched by CNO nucleosynthesis, during the second dredge-up (hereinafter SDU) episode, occurring after the core He-burning phase. The helium enrichment is higher the more massive is the star; the largest helium mass fractions,  $Y \sim 0.37$ , are achieved by stars of initial mass  $\sim 8 M_{\odot}$  (Ventura 2010).

An important feature of the evolution of this class of stars is the off-center ignition of carbon burning in condition of partial degeneracy. The consequent development of a convective flame, propagating inwards, favors the formation of a degenerate core, composed of oxygen and neon (García-Berro & Iben 1994; García-Berro et al. 1997; Ritossa et al. 1996; Siess 2006, 2007, 2010). The thermally pulsing phase of these stars is commonly referred to as Super Asymptotic Giant Branch (SAGB) evolution.

The pollution from SAGB stars in low-metallicity environments, such as GC, is not completely understood. There is a general consensus that the gas ejected by these objects is enriched in helium, because most of the helium increase at the surface takes place in the evolutionary phases previous to the beginning of thermal pulses (hereinafter TP).

Regarding the other chemical species, particularly the light elements involved in the correlation/anti-correlation patterns observed in GC stars, the yields are sensitive to the details of modelling of the TP phase, particularly to the description of mass loss, the efficiency of mixing at the base of the envelope and the strength of HBB. An exhaustive discussion on this argument, with the role played by different physical mechanisms, is given in Doherty et al. (2014) and it will be investigated in the next section.

### 3 NGC 2808: A CORNERSTONE IN THE UNDERSTANDING OF MULTIPLE POPULATIONS IN GC

In the context of the self-enrichment process by AGB stars, D’Antona et al. (2016, hereafter D16) proposed a temporal sequence for the formation of the five populations belonging to NGC 2808 (see Fig.1), which can be summarized as follows: a) the FG of the cluster defines the group P1(B in D16); b) regarding the SG, the stars with the most extreme chemical composition (group E) formed within  $\sim 20$  Myr from the end of the epoch of type II SNe explosions, directly from the gas ejected by SAGB stars; c) the remaining SG stars (groups I2, I1 and P2) formed later, from the gas lost by AGB stars of lower mass ( $4 - 6 M_{\odot}$ ), diluted with pristine matter.

For the reasons discussed in the previous section, the reliability of this understanding can be assessed via the analysis of the chemical composition of stars in group E: because no dilution occurred when these stars formed, it is crucial

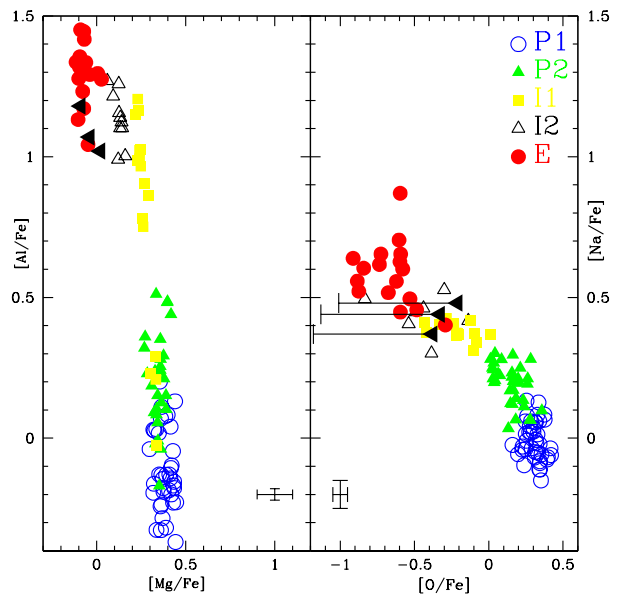


**Figure 1.** Abundance ratios  $[Al/Fe]$  and  $[Na/Fe]$  as a function of  $[Mg/Fe]$  and  $[O/Fe]$  respectively in RGB stars of NGC 2808 measured by Carretta et al. (2015) and Carretta et al. (2018). Different colours indicate the five populations as defined in Carretta (2015) using the Mg-Na plane. Large and black triangles are the yields computed in this work for AGB stars of  $M=6.5, 7.0$  and  $7.5 M_{\odot}$  (see also Table 1). In the case of Oxygen the uncertainties related the adopted extra-mixing (see text) is also displayed.

that the SAGB yields correspond to the chemical patterns traced by these objects. Compared to D16 we can make a significant step forward in this direction, because that work does not include the discussion of the abundances of aluminum and silicon. These elements are of paramount importance to interpret the observations, because, unlike CNO elements and sodium, their surface abundance does not change during the RGB evolution, thus the observations reflect the original chemical composition of the stars.

Carretta et al. (2018) show that group E stars exhibit the most extreme chemical composition, for all the species observed. Indicating with  $\delta X = [X/Fe]_E - [X/Fe]_{FG}$  the differences between the surface mass fraction of the species  $X$  for group E and FG stars (P1 according their nomenclature), Carretta et al. (2018) (see Table 6 and Fig. 1) find  $\delta Na \sim +0.6$ ,  $\delta Mg \sim -0.4$ ,  $\delta Al \sim +1.5$ ,  $\delta Si \sim +0.2$ .

The situation for oxygen is more complex, because the observations indicate for E stars  $-1.5 < \delta O < -0.7$ , an excursion which is significantly larger than the expected scatter ( $\sim 0.1$ ) and also larger than the one observed in the FG. We will discuss this point in the next section.

These recent results make appropriate a revision of the scenario given in D16 and/or the SAGB models used in that work. First of all in the SAGB models by Ventura et al. (2013) used by D16 to interpret the abundance patterns of E stars in NGC 2808, with the sole exception of helium, the most contaminated gas is produced by stars of initial mass  $\sim 6 M_{\odot}$  while the SAGB yields of O, Mg, Al and Si are not significantly altered with respect to the original

<sup>1</sup> The exact values of the mass depend on the adopted metallicity and on the assumptions regarding the extent of the extra-mixing from the border of the convective core during the core H-burning phase. When no overshooting is considered, the above range in mass would shift upwards to  $9 - 10 M_{\odot}$

chemistry (see Fig. 6 in Ventura et al. 2013). In particular D16 remarked that the Ventura et al. (2013) models correctly predict Mg depletion in group E, but their Mg abundances are  $\sim 0.15$  dex larger than those observed, as recently noticed also by Carretta et al. (2018) so further exploration is needed to re-evaluate the Mg case.

They also suggested that the small oxygen measured in same E stars could be explained with deep mixing during the RGB phase, an hypothesis that will be tested in this work through the computation of specific models.

In the following section we present new SAGB models, calculated on purpose to explain stars belonging to group E in NGC 2808, we will check in this work to check whether the models are consistent with the observations.

## 4 SAGB MODELLING

### 4.1 Chemical and physical input

To study the extreme population of E stars in NGC 2808 we calculated ad hoc SAGB models with initial mass in the range  $6.5 - 8 M_{\odot}$ . The chemical composition is the same as the FG of the cluster, i.e. the stars belonging to group P1 in Carretta et al. (2018). The initial abundances of O, Na, Mg, Al and Si, reported in Table. 1, were chosen accordingly. For carbon and nitrogen we assumed solar-scaled abundances, with  $[C/Fe] = [N/Fe] = 0$ . With these choices, the metallicity corresponding to the average  $[Fe/H] \sim -1.15$  measured by Carretta et al. (2018) is  $Z = 2 \times 10^{-3}$ . The initial helium was taken as  $Y = 0.25$ .

We used the same physical ingredients described in detail in Ventura & D’Antona (2009). We briefly recall here the most relevant input.

*Convection.* Convection was modelled according to the Full Spectrum of Turbulence (hereinafter FST) model, developed by Canuto & Mazzitelli (1991). Nuclear burning and mixing of chemicals are treated simultaneously, according to the diffusive schematization by Cloutman & Eoll (1976). During the core burning phases we assumed overshoot from the border of the convective core, modelled via an exponential decay of the convective velocities within the radiatively stable zones, with an e-folding distance  $\zeta = 0.02 \times H_P$  (Ventura et al. 1998). No extra-mixing was assumed during the TP phase.

*Nuclear reactions.* We used the NACRE compilation (Angulo et al. 1999) for the cross sections of the various reactions included in the nuclear network. The exceptions are:  $^{14}\text{N}(p, \gamma)^{15}\text{O}$  (Formicola et al. 2004);  $^{22}\text{Ne}(p, \gamma)^{23}\text{Na}$  (Hale et al. 2002);  $^{23}\text{Na}(p, \gamma)^{24}\text{Mg}$  and  $^{23}\text{Na}(p, \alpha)^{20}\text{Ne}$  (Hale et al. 2002). For what attains the rate of the proton capture reactions by the heavy Mg isotopes we used the same input as in Ventura et al. (2018), which allowed us to reproduce the Mg-Al trends observed in M13, NGC6752 and NGC2419.

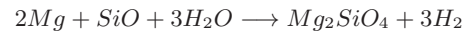
*Mass loss.* We follow the description by Blöcker (1995) to model mass loss during the TP phases. This treatment provides a numerical fit of  $\dot{M}$  as a function of mass and luminosity of the star, based on hydrodynamic models of

O-rich envelopes, in which mass loss is driven by radiation pressure on the dust particles formed in the circumstellar envelope. In agreement with our previous works, in the initial TP phases we assume the free parameter entering the Blöcker (1995) formula  $\eta_R = 0.02$ , in agreement with the calibration based on the luminosity function of Li-rich stars in the Magellanic Clouds, given in Ventura et al. (2000). However, in the present investigation we propose an innovative approach, that considers the change in the amount of dust formed, as a consequence of the alteration of the surface chemical composition of the star.

In the circumstellar envelope of O-rich, AGB (and SAGB) stars, the most relevant dust species are alumina dust and silicates (Ferrarotti & Gail 2006; Ventura et al. 2014). Under HBB conditions, the presence of these particles, owing to the large luminosities experienced, triggers a significant acceleration of the stellar wind, even in metal-poor environments (Di Criscienzo et al. 2013).

Because alumina dust is extremely transparent to the electromagnetic radiation, the acceleration of the wind is mainly due to silicates and, more specifically, to iron-free olivine, a compound including magnesium, silicon and oxygen atoms, whose formula is  $\text{Mg}_2\text{SiO}_4$ .

The reaction leading to the formation of iron-free olivine is (Ferrarotti & Gail 2006)



Given the extreme stability of the CO molecules, only the oxygen not locked into CO is available to form dust; therefore, the quantity of dust which forms depends also on the number of carbon particles. The rate with which the reaction above proceeds is determined by the addition of Mg atoms, or by the addition of SiO molecules, or by the supply of oxygen by water molecules. Therefore, the rate of the silicates growth is proportional to the least (in number) among magnesium, silicon and oxygen, which is called "key element".

In the present work we kept  $\eta_R$  constant until the number density of the key element is unchanged. We will see in section 4.4 that this holds only in the initial phases, before the destruction of magnesium determine a significant decrease in the rate of dust formation and for this reason we assumed that  $\eta_R$  scales with the abundance of the key element after the beginning of Mg destruction till the achievement of the C-star phase after which we kept the mass loss rate constant until the consumption of the whole envelope. Note that the above correction is required only when extremely strong HBB conditions are activated; in stars of lower mass and, more generally, in higher metallicity stars, the surface magnesium is not consumed severely, thus dust is formed efficiently for the whole TP evolution.

### 4.2 The pre-TP evolution

The evolutionary phases following the end of core helium burning and before the beginning of TP of stars undergoing the SAGB evolution are characterized by the inwards penetration of the convective envelope and the ignition of carbon burning.

The left panel of Fig. 2 shows the variation of the position of the base of the surface convective zone and of the



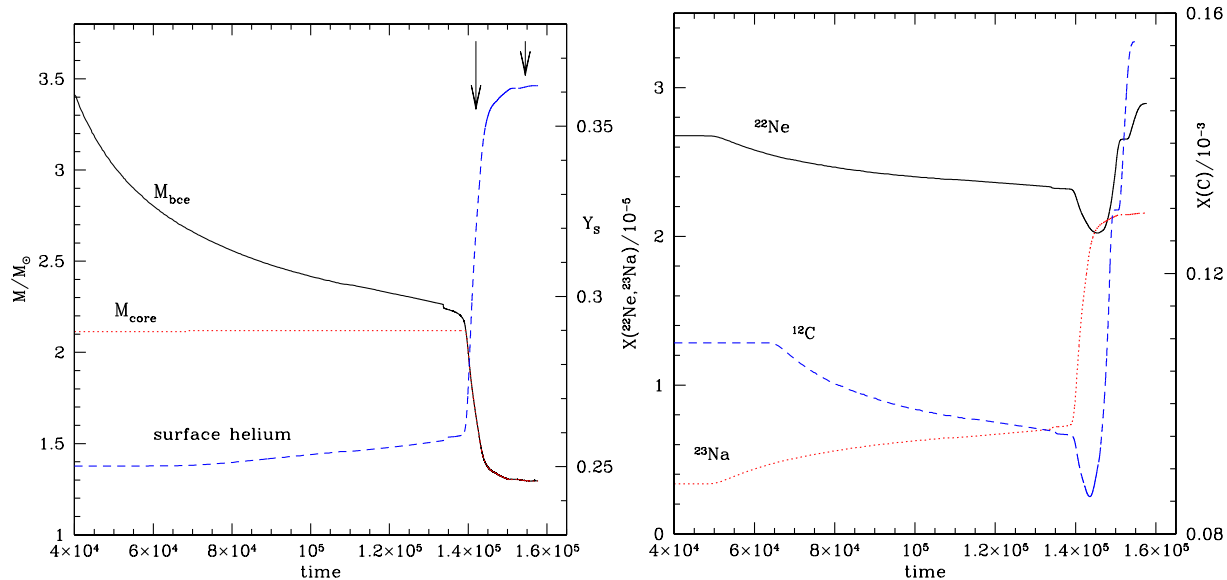


**Figure 2.** Left: The evolution of the mass of the base of the envelope (solid, black line) and of the core mass (dotted, red) of a  $7.5 M_{\odot}$  model, during the evolutionary phases following the exhaustion of central helium and before the beginning of thermal pulses. Times are counted since the end of central helium. The vertical arrows indicate the times of the ignition of the first episode of carbon burning (arrow on the left) and of the formation of the O-Ne core (right). The dashed, blue track indicate the surface helium abundance (scale on the right). Right: The evolution of the surface mass fraction of  $^{22}\text{Ne}$  (solid, black lines) and sodium (dotted, red) in the same evolutionary phases shown in the left panel. The behaviour of the surface carbon (dashed, blue line, scale on the right) is also shown.

helium-hydrogen interface in the model of (initial) mass  $7.5 M_{\odot}$ . In the final part of this phase the base of the envelope reaches the chemical discontinuity, starting the second dredge-up (SDU); the surface convection pushes the H/He boundary inwards, by  $\sim 1 M_{\odot}$ , and reaches stellar regions enriched in helium and, more generally, contaminated by nuclear activity.

As indicated by the left arrow in the figure, the first ignition of carbon burning occurs shortly after the beginning of the SDU. The formation of the O-Ne core (right arrow), towards the end of the second ignition of carbon, takes place when the SDU is practically finished.

We see that the occurrence of SDU determines a significant increase in the surface helium, whose mass fraction is raised by 0.11. This result is extremely robust, because even in case of a more efficient SDU the increase in the surface helium would remain substantially unchanged: indeed in this case the base of the envelope would reach layers of the star enriched in carbon, where helium burning occurred. The present results are in agreement with the investigation by Doherty et al. (2014), who studied the SAGB evolution of stars of similar metallicity.

The right panel of Fig. 2 shows the variation of the surface abundances of  $^{12}\text{C}$ ,  $^{22}\text{Ne}$  and  $^{23}\text{Na}$  during the same phases shown in the left panel. An important phenomenon taking place during these phases is the formation of a convective region in the helium burning shell, which eventually merges with the penetrating envelope (Iben et al. 1997; Siess 2007). The signature of this convective episode can be seen in the behaviour of the surface carbon: while in the phases following the beginning of SDU the surface  $^{12}\text{C}$  decreases, towards the end of SDU the amount of carbon in the envelope increases, because the external convective region reaches layers touched by helium burning.

A further consequence of the deep penetration of the convective envelope, very important for the present investigation, is the increase in the surface  $^{22}\text{Ne}$ , whose behaviour is qualitatively similar to carbon. During the first part of SDU the surface  $^{22}\text{Ne}$  decreases, as in the regions mixed with the surface  $^{22}\text{Ne}$  was exposed to proton capture, which synthesized sodium. In the last part of SDU the surface  $^{22}\text{Ne}$  increases, because the surface convection reaches regions of the star where repeated  $\alpha$  captures favoured a significant synthesis of  $^{22}\text{Ne}$ , now transported to the surface. During the SDU the sum  $^{22}\text{Ne} + ^{23}\text{Na}$  increases by 70%; this will be extremely important for the sodium content of the ejecta, considering that almost the totality of the  $^{22}\text{Ne}$  in the envelope is converted into sodium during the TP phase.

The other two species touched by SDU (not shown in Fig. 2 for clarity reasons) are oxygen, whose surface content decreases by  $\sim 25\%$  (the oxygen abundance changes from 0.0016 to 0.0009) and nitrogen, which increases by a factor  $\sim 7$  (from  $X(\text{N}) = 4.98 \times 10^{-5}$  to  $X(\text{N}) = 3.5 \times 10^{-4}$ ).

### 4.3 The thermally pulsing phase

The envelope of SAGB stars is lost almost entirely during the TP phase. Although extremely short, this is the evolutionary phase most important for the feedback from these objects to the interstellar medium, as it is now that most of the gas and dust pollution occurs.

We show in Fig. 3 the variation of the surface chemical composition, in terms of the surface abundances of the CNO elements, sodium, and the species involved in the Mg-Al-Si nucleosynthesis. The figure refers to the same model, of initial mass  $7.5 M_{\odot}$ , shown in Fig. 2. We report the current mass of the star on the abscissa, to have a better idea of the chemistry of the gas ejected.

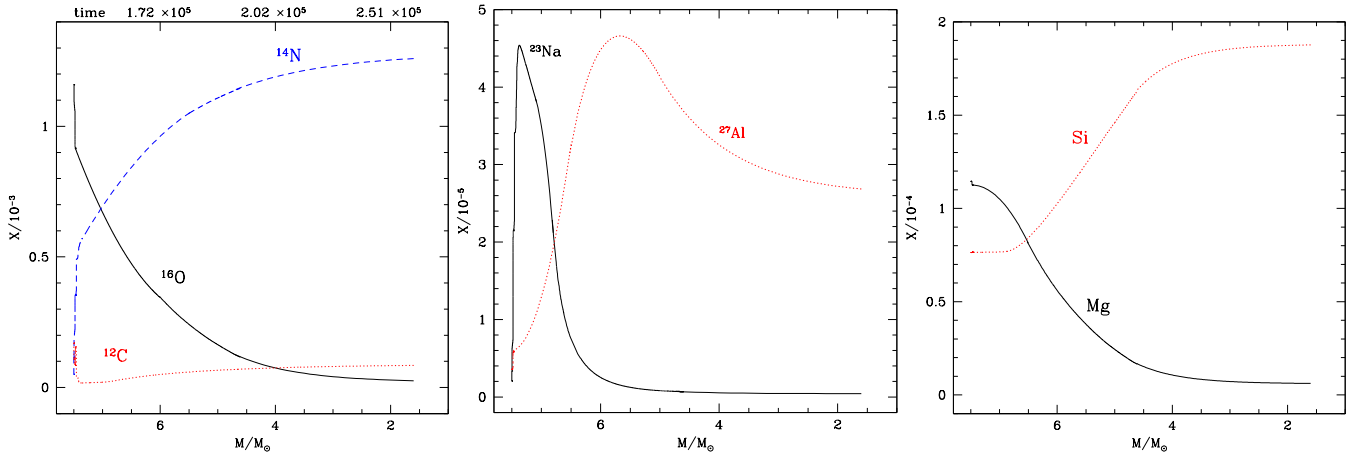


**Figure 3.** The evolution of the surface chemical composition of the  $7.5 M_{\odot}$  model shown in Fig. 2, during the TP phase. The mass fractions of the CNO elements is shown in the top, left panel, whereas the abundances of sodium and aluminium are reported in the top, right panel and those of magnesium and silicon in the bottom, left panel.

Massive AGB stars are characterized by strong HBB, since the early TP stages (Ventura & D’Antona 2011). This holds even more in metal-poor environments (Ventura et al. 2013). In the model reported in Fig. 3 the temperature at the base of the envelope is slightly higher than 110 MK at the beginning of this phase and increases gradually during the following evolution, up to  $\sim 140$  MK. Under these conditions the internal regions of the envelope experiment a very advanced p-capture nucleosynthesis.

As shown in the left panel of Fig. 3, the CNO species subject to the most significant alterations are nitrogen, which increases by a factor of  $\sim 4$  with respect to the post-SDU abundance, and oxygen, which is almost entirely consumed. This behaviour is a clear signature of the activation of the full CNO cycling at the base of the envelope. The carbon trend is slightly increasing during this evolutionary phase, because the carbon equilibrium abundance is higher the larger is the temperature at which CNO nucleosynthesis takes place.

The central panel of Fig. 3 shows that the Ne-Na nucleosynthesis is efficiently activated since the beginning of the TP phase. The behaviour of sodium under HBB conditions was addressed in details by Mowlavi (1999) and further tested in FST-based AGB models by Ventura & D’Antona (2006). The present findings confirm on the qualitative side the results from these earlier investigations, with the difference that in this case the accumulation of  $^{22}\text{Ne}$  in the envelope, favored by efficient SDU, leads to a generally larger synthesis of sodium. The sodium mass fraction during the initial TP-AGB phases reaches values  $\sim 10$  times higher than in the matter from which the star formed. After reaching a maximum, the abundance of sodium begins a negative trend, because the destruction channels, particularly the  $^{23}\text{Na}(p, \gamma)^{24}\text{Mg}$  reactions, becomes more dominant with respect to sodium production the higher is the temperature.

The ignition of the Mg-Al-Si nucleosynthesis is witnessed by the behaviour of magnesium, silicon (shown in the right panel of Fig. 3) and of aluminium (middle panel). The development of this nuclear channel is rather complex, because the total magnesium is split into three isotopes, each exposed to proton capture. The interplay among the various

reactions was investigated in detail by Arnould et al. (1999), while an exhaustive application to SAGB modelling is given in Siess & Arnould (2008). In a recent work Ventura et al. (2018) investigated the role of the various cross-sections on the results obtained. The destruction of  $^{24}\text{Mg}$ , the most abundant isotope, begins shortly after the activation of the Ne-Na nucleosynthesis, and continues efficiently for the whole TP phase, until  $^{24}\text{Mg}$  is almost exhausted.  $^{25}\text{Mg}$  and  $^{26}\text{Mg}$  are produced in the initial phases, then they are destroyed by proton capture. The total Mg decreases steadily during the TP phase, until reaching final abundances below 10% of the original value.

The destruction of magnesium favors the production of aluminium and silicon. The behaviour of Al is not monotonic with time. Initially the surface aluminium increases up to values ten times higher than the initial content; in the final part the surface Al decreases, owing to the higher and higher efficiency of the  $^{27}\text{Al}(p, \gamma)^{28}\text{Si}$  reaction, which favours a significant increase in the surface silicon.

#### 4.4 Mass loss: the big unknown of the SAGB phase

While it is generally recognized that strong HBB takes place in SAGB models (Siess 2010; Doherty et al. 2014, 2015), the description of mass loss is still under debate and largely unknown. The main issue in this context is that the mechanism favoring mass loss during the TP-AGB phase is still poorly known.

The impact on the treatment of mass loss on the physical evolution of SAGB stars, on the determination of the initial-final mass relationship and on the chemical yields are discussed in Doherty et al. (2014, 2015).

In the previous works on this argument we calculated  $\dot{M}$  via the Blöcker (1995) description (Ventura & D’Antona 2011; Ventura et al. 2013), using the calibrated parameter  $\eta_R = 0.02$  for the whole TP phase. A consequence of this choice was that the gas ejected by SAGB models of mass  $7 - 8 M_{\odot}$  is on the average less processed than in the lower mass counterparts, because the mass loss rates were so large that the rate at which the envelope is lost is faster than

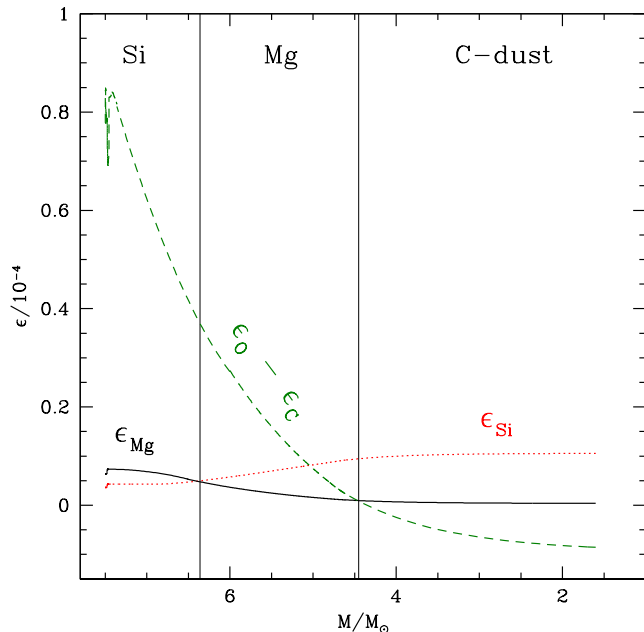


**Figure 4.** The number densities (relative to the hydrogen particles) of magnesium (black solid), silicon (red dotted) and of the oxygen excess (green dashed) with respect to carbon at the surface of a  $M=7.5 M_{\odot}$ . The three temporal phases are highlighted in each of which the behavior of mass loss is governed by the abundance of Si, Mg C, respectively (see text).

the pace of the p-capture reactions. This general behaviour holds for all the chemical species but helium, whose surface content, as discussed earlier, is mainly determined by SDU.

As discussed in section 4, we now reconsidered this choice, to account for the effects of the radiation pressure on dust particles. To understand how this affects the SAGB modelling, we show in Fig. 4 the evolution of the surface number densities of the potential key elements for dust formation, namely silicon, magnesium, and of the difference between the oxygen and carbon; for each element  $X$  we plot the quantity  $\epsilon(X) = n(X)/n(H)$ , i.e. the surface number density, relatively to hydrogen (Ferrarotti & Gail 2006).

During the initial TP-AGB phases the key element, determining the dust formation rate, is silicon, which is the least abundant among the species relevant to the formation of silicates; this situation is maintained until the mass of the star decreases down to  $\sim 6.5 M_{\odot}$ . During this phase we expect that the mass loss rate increases, owing to the simultaneous increase in the luminosity of the star and in the silicon content of the envelope; this is in agreement with the results obtained using the Blöcker (1995) recipe, which is characterized by a steep dependence on the luminosity. In the following phases magnesium replaces silicon as the key element to dust formation (see Fig. 3); this is due to the destruction of magnesium and the synthesis of silicon by HBB, which eventually makes the number of Mg particles smaller than Si. Because the surface density of the key species is now diminishing, less and less dust will be formed, with the consequent decrease in the rate of mass loss (requiring use of a smaller  $\eta_R$ ). We used this description until the  $C/O$  ratio exceeds unity entering in the C-star phase, when the mass of the star drops below  $\sim 4.5 M_{\odot}$  in Blöcker

(1995); after which we kept the mass loss rate constant until the consumption of the whole envelope. The latter choice is somewhat arbitrary, but it has practically no effects on the gas yields.

It is also possible that mass loss driven by radiation pressure is resumed after a while, now stimulated by the carbon dust grains formed.

## 5 DISCUSSION

Table1 reports the yields of SAGB stars of initial mass 6.5, 7, 7.5  $M_{\odot}$ . The table includes the average chemical composition of FG stars and of SG stars belonging respectively to group P1 and E of NGC 2808 (see also Fig. 1).

### 5.1 Direct influences of HBB: Magnesium depletion and Silicon enrichment

Magnesium and silicon provide a direct information regarding the capability of the present AGB models to reproduce the chemistry of SG stars, because their behaviour during the TP phase is monotonic (see Fig. 3).

Mg is subject to destruction via p-capture: in the early TP phases  $^{24}\text{Mg}$  is destroyed in favour of  $^{25}\text{Mg}$  and  $^{26}\text{Mg}$ , whereas in the more advanced TP evolution the heavier Mg isotopes are also exposed to efficient p-capture, which determines a fast decrease in the overall surface magnesium. In the present SAGB models we find that the magnesium in the ejecta is  $[Mg/Fe] = 0$ , 2.5 times smaller than FG stars.

Silicon is synthesized by p-capture on Al nuclei. The production of silicon requires not only that Mg burning is activated, but also that the process is sufficiently fast to allow the accomplishment of the whole Mg-Al-Si chain on time scales shorter than (or comparable to) the evolutionary time scale; this requires large HBB temperatures, in excess of 100 MK. In the present computations, as reported in Table.1, we find that the silicon in the ejecta is  $[Si/Fe] = +0.4$ , to be compared with the quantity measured in FG stars, i.e.  $[Si/Fe] = +0.25$

### 5.2 HBB equilibria: the behaviour of Aluminium and Sodium

We find a significant Al enrichment in the ejecta, by a factor  $\sim 10$  ( $[Al/Fe] \sim 1$ ). As discussed in section 4.3, the Al content of the envelope during the TP evolution is determined by the equilibrium between the production and the destruction channels, thus the results are extremely sensitive to the cross-section of the  $^{27}\text{Al}(p,\gamma)^{28}\text{Si}$  reaction: the comparison with the Al measured in E stars seems to require slightly lower rates, but the differences are not sufficiently significant to require a supplementary analysis on this argument.

Sodium is the most delicate species entering this discussion, because the surface abundance reflects the equilibria between the production and the destruction mechanisms (see Section 4.3), both very sensitive to the temperature, thus exposed to significant variation during the TP phase. This explains the TP evolution of the surface sodium, shown in the top, right panel of Fig. 3. As reported in Table1, the average sodium of the ejecta,  $[Na/Fe] \sim 0.5$ , is similar to

**Table 1.** Average abundances of proton-capture elements in the extreme population E of NGC 2808 taken from Table 6 of Carretta et al. (2018) compared with the yields derived for SAGB of different masses.

	Y	[C/Fe]	[N/Fe]	[O/Fe]	[Na/Fe]	[Mg/Fe]	[Al/Fe]	[Si/Fe]
NGC 2808 stars								
FG (P1)	-	-	-	$0.308 \pm 0.058$	$-0.005 \pm 0.067$	$0.384 \pm 0.041$	$-0.114 \pm 0.141$	$0.265 \pm 0.026$
SG (E)	-	-	-	$-0.656 \pm 0.161$	$0.592 \pm 0.112$	$-0.050 \pm 0.050$	$1.292 \pm 0.113$	$0.390 \pm 0.036$
SAGB yields								
$M/M_{\odot}$	Y	[C/Fe]	[N/Fe]	[O/Fe]	[Na/Fe]	[Mg/Fe]	[Al/Fe]	[Si/Fe]
6.5	0.36	-0.62	1.33	-0.38	0.37	-0.09	1.18	0.44
7	0.36	-0.60	1.33	-0.33	0.44	-0.04	1.07	0.48
7.5	0.37	-0.51	1.29	-0.21	0.48	0.02	1.02	0.42

the quantity observed in E stars. Despite the vigorous destruction of sodium in the advanced TP phases, the ejecta are enriched in sodium (by a factor  $\sim 3$ ), because during the initial part of the evolution the sodium in the envelope reaches abundances 10 – 20 times higher than in the matter from which the star formed; this can be clearly seen in the top, right panel of Fig. 3. Such a large increase in the surface sodium is partly due to the accumulation of  $^{22}\text{Ne}$  during the SDU (see discussion in section 4.2); an additional motivation is that the sodium enrichment of the envelope takes place during the initial TP phases, when dust production is at the maximum efficiency (region labelled as Mg in the bottom, right panel of Fig. 3): this favours the release of large quantities of sodium-rich gas into the interstellar medium.

### 5.3 Can we obtain oxygen-free ejecta?

Oxygen deserves a separate discussion. The SAGB yields reported in Table 1 have  $[O/Fe] \sim -0.2$ ,  $\sim 4$  times smaller than FG stars. On the other hand, Fig. 1 above and Fig. 3 in Carretta et al. (2018) show that some stars belonging to group E have extremely low surface oxygen, up to 20 times lower than observed in FG stars; furthermore, some of these measurements are upper limits.

We did several tests, by varying the HBB modelling and the description of mass loss: our conclusion is the impossibility of producing SAGB ejecta with such low oxygen contents. The only possibility is that the stars suffer extremely low mass loss during the initial TP phases, until most of the oxygen in the envelope is consumed, via p-capture. The rate of mass loss required to accomplish this task should be below  $10^{-6} \dot{M}/\text{yr}$ , far too small for this high luminosity, expanded stars. In this case the overall agreement between the yields of SAGB stars and the chemistry of E stars would be substantially worse, because the gas ejected would be practically sodium free and would show magnesium depletion and silicon enrichment far in excess of the quantities observed.

On the other hand it is not possible to reproduce all the oxygen abundances of E stars at the same time, given the large spread observed, amounting to almost 1 dex. Oxygen is very peculiar on this side, because Carretta et al. (20018) show that the range of measured values is much wider than the intrinsic error,  $\sim 0.1$  dex. However the yields of

the SAGB stars used here are compatible with the largest oxygen abundances among E stars.

### 5.4 Mixing on the RGB

This difficulty of HBB to account for the most extreme O-depletion cases was already clear a decade ago, as a very extended O–Na anticorrelation was already shown by NGC 2808 giants (Carretta et al. 2006) and by M 13 giants (Snedden et al. 2004). In this context, D’Antona & Ventura (2007) proposed to explain it by extramixing during the giant stage, due to rotational evolution of the stars born with the extreme anomalous composition provided by the AGB ejecta.

The stars we are analyzing are also extremely helium-rich (see Table 1), and during the evolution they do not develop the strong molecular weight barrier which prevents rotational mixing. For this reason, the first generation giants, born with primordial initial helium content, even if born with a similar rotational spread, would not be subject to the same kind of rotational mixing, and would not display a similar oxygen spread. Deep mixing, during which the bottom of the envelope penetrates down until reaching the more internal regions of the H-burning shell, where CNO cycling had been active, was first invoked by Denisenkov & Denisenkova (1990) to explain results from high resolution spectroscopy of RGB stars in  $\omega$  Centauri. We suggest now that this is a plausible explanation for the minimum oxygen abundances, and possibly also for the star-to-star differences in the E population of NGC 2808 as given in Carretta et al. (2018). We studied the evolution of stars now evolving in the cluster, and formed with the composition of the SAGB ejecta of the  $7.5 M_{\odot}$ , i.e.  $[O/Fe] = -0.2$  and  $Y=0.37$  (see Table 1), assuming that, during the RGB phase, are exposed to non canonical extra-mixing, which favours a further depletion in the surface oxygen, but leaves the other elements signature of second generation, such as sodium and magnesium, unaltered. Because the gas is enriched in helium, these stars evolve faster than FG stars: consequently, for a given age, the mass currently evolving through the RGB is lower. Assuming a 12 Gyr age for NGC 2808, a star formed directly from the SAGB winds, and nowadays experiencing the RGB evolution, has a mass of  $0.65 M_{\odot}$ .



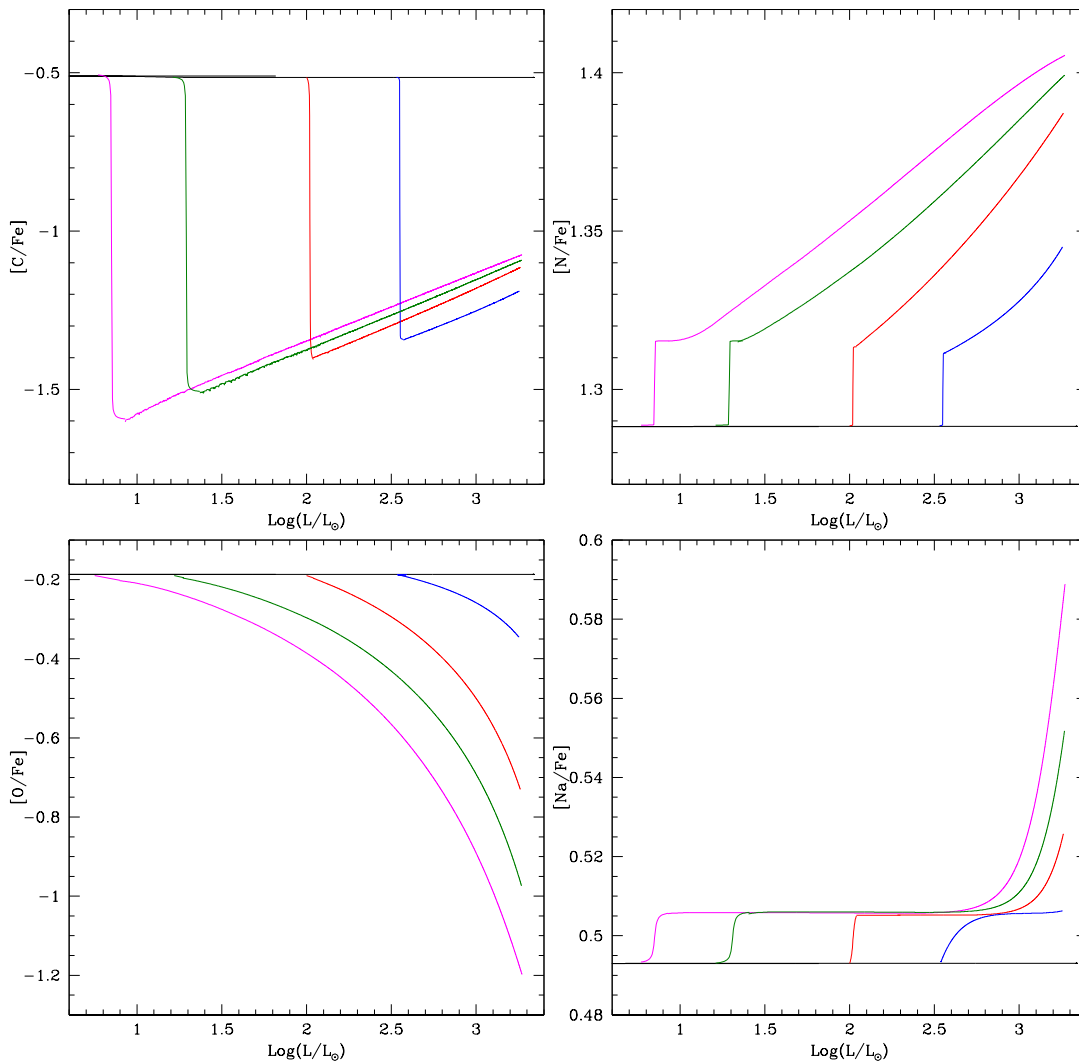


**Figure 5.** The variation of the surface mass fractions of the CNO elements and of sodium during the RGB evolution of models of mass  $0.65 M_{\odot}$  calculated with the same chemical composition of the SAGB ejecta. The horizontal, black tracks refer to the model calculated with canonical convective mixing, whereas the sequence of magenta, green, red and blue lines refer to models where deep mixing was assumed starting from different evolutionary stages during the RGB ascending.

We calculated various evolutionary sequences of  $0.65 M_{\odot}$  models, with the chemical composition of the SAGB ejecta reported in Table 1. We assumed non canonical, deep mixing, started at different stages of the RGB phase, and prosecuted until the helium flash. To model such mixing we assumed that the surface convective zone penetrates inwards, down to regions whose temperature is  $\Delta \log T = 0.05$  hotter than the formal border, fixed by the Schwarzschild criterion. In the extra-mixed zone we assumed the exponential decay of the convective velocities, as described in section 4.1. The results are shown in Fig. 5, where the variation of the surface abundances of the individual species are shown as a function of the luminosity of the star. We do not show the behaviour of Mg, Al and Si, because no variation in the surface mass fractions of these elements is found.

The top, left panel of Fig. 5 shows that deep mixing causes a decrease in the surface carbon, whose initial abundance is  $\sim 3$  times smaller than FG stars. Note that after

the initial, dramatic drop in the carbon content, the  $^{12}\text{C}$  mass fractions starts to increase, because the base of the envelope reaches layers touched by full CNO cycling, where the equilibrium  $^{12}\text{C}$  is higher than in CN burning regions.

The surface nitrogen, shown in the top, right panel of Fig. 5, is subject to a modest increase, below 0.1 dex. The reason for this behaviour is that the initial N is almost 20 times higher than in FG stars, which leaves little room for a further, percentage increase in the N content (note that the quantity reported on the y-axis is in logarithmic scale).

We see in the bottom, left panel of Fig. 5 that oxygen is exposed to significant alteration during the RGB ascending. The gradual penetration of the surface convection, down to regions of the star touched by CNO nucleosynthesis, determines a progressive reduction of the surface oxygen, which can be depleted by a factor  $\sim 10$  during the RGB phase (note that the initial oxygen was 4 times smaller than FG stars).

The behaviour of sodium, shown in the bottom, right

panel of Fig. 5, is qualitatively similar to nitrogen. Despite the surface convection reaches zones involved in Ne-Na nucleosynthesis, the  $^{22}\text{Ne}$  available is extremely small and the initial sodium is 3 times higher than in FG stars; these conditions prevent a significant, percentage increase in the sodium content, thus  $[\text{Na}/\text{Fe}]$  raises by less than 0.1 dex.

### 5.5 Understanding the most contaminated stars in NGC 2808

The discussion in section 3 outlined the importance of NGC 2808 for the comprehension of the formation of multiple populations in GC. We stressed how important is the interpretation of the stars with the most extreme chemical composition (E stars, in Carretta et al. 2018), to understand whether self-enrichment by AGB stars might explain the chemical abundances observed: it is essential that the chemical composition of these stars are in agreement with the ejecta from SAGB stars. Fig. 1 shows the comparison between the yields of the SAGB models discussed here and the chemical composition of E stars in the O-Na and Mg-Al planes.

The magnesium depletion ( $\delta Mg = -0.4$ ) and the silicon enrichment ( $\delta Si = +0.2$ ) reported in Table 1 are in nice agreement with the observations: this is a confirmation that the HBB temperatures are sufficiently hot to allow the nucleosynthesis required to favours the destruction of the magnesium isotopes and the synthesis of significant quantities of silicon<sup>2</sup>.

The aluminium and sodium abundances of E stars are also in good agreement with the chemistry of the SAGB ejecta. This finding indicates that the interplay of HBB and mass loss during the SAGB phase is appropriate to allow the required enrichment in Na and Al. Sodium is particularly indicative on this side, because its behaviour is subject to significant changes during the TP phase: producing gas enriched in sodium requires a strong mass loss during the initial TP phases, when the surface regions of the stars are characterized by large sodium abundances.

The nucleosynthesis at which the base of the envelope is exposed favours the release of oxygen-poor gas. As shown in Fig. 1, we find that the average oxygen in the SAGB ejecta is  $[O/Fe] = -0.2$ , consistent with the largest abundances measured in stars in group E. To explain the most extreme Oxygen abundances measured in He-Extreme stars we propose that deep mixing occurs during the RGB evolution. This would be, in principle, the consequence of the chemical mixing associated with angular momentum evolution of initially rotating stars. The large spread in these values may be imputed to different reasons. First of all, the stars with the smallest oxygen content may be those into which deep mixing started earlier during the RGB evolution, as displayed in Figure 3; another possibility is that the stars were born with somewhat different AGB yields for oxygen (as displayed in Table 1) and they suffer a similar extramixing, but end up with a different surface oxygen.

<sup>2</sup> We remark here that silicon is among the most abundant species, among the various elements: an increase in the surface silicon of +0.2 dex indicates that significant amounts of magnesium (and aluminium) are converted into silicon

## 6 CONCLUSIONS

We investigate the formation of multiple populations in the globular cluster NGC 2808. On the wake of previous explorations, we focus on the possibility that the SGs formed with the contribution of the gas ejected by the progeny of stars of mass  $4 M_{\odot} < M < 8 M_{\odot}$ , during the AGB phase.

This analysis is extremely timely, because recent data from high resolution spectroscopy present a complete overview of the chemical composition of dozens of FG and SG stars in the cluster, making available the individual abundances of all the light elements: oxygen, sodium, magnesium, aluminium and silicon.

These observational results offer an unprecedented opportunity of constraining the physical conditions and the degree of nucleosynthesis at which the contaminated gas, from which SG stars formed, was exposed. This is particularly important for the AGB self-enrichment scenario, which we discuss here, because according to this hypothesis the stars with the most contaminated chemistry should have the same chemical composition of the most massive stars escaping type II SNe explosion, i.e.  $6.5 - 8 M_{\odot}$  stars, undergoing the SAGB evolution.

We present new models for massive AGB stars, evolved from the same chemical composition of the stars belonging to the FG of the cluster. We propose a modification of the mass loss description used in previous works, to consider the decrease in the effects of the radiation pressure, when magnesium is destroyed by HBB at the base of the envelope.

Our results show that the present models nicely reproduce the depletion of magnesium and the enrichment in aluminium and silicon observed in the most contaminated stars. Furthermore, unlike previous explorations, the predictions from this modelling can nicely reproduce the sodium enrichment observed, despite the intense sodium destruction occurring in the advanced AGB phases. This agreement is due to the combined effects of: a) the accumulation in the envelope of  $^{22}\text{Ne}$ , synthesized in the regions exposed to  $3\alpha$  nucleosynthesis, which occurs during the second dredge-up; b) the strong mass loss suffered by these stars during the phase with the maximum enrichment in sodium.

The large spread in the oxygen abundances is explained by invoking deep mixing during the RGB phase. The stars with the largest oxygen  $[O/Fe] = -0.2$ , in agreement with the results from SAGB modelling, did not suffer any extramixing; conversely, the stars with the lowest abundance of oxygen are those exposed to deep mixing since the early RGB phases.

Concluding we agree with Carretta et al.(2018) that NGC 2808 is one of the best benchmark to test any scenario for the origin and the evolution of multiple populations in GC but we are not equally in agreement with the fact that large inconsistencies, related to the nucleosynthesis exist when the temporal sequence for the formation of the various populations is formulated within the self-enrichment scenario by massive AGB. In particular, in this work the extreme He-rich population allows us to test AGB scenario focusing on the role of very massive AGB stars. In this evolutionary phase the great unknown is the mass loss, but we have shown that a Blocker's approach with a calibration that takes into account the variation of Mg during the evolution in AGB nicely reproduces the observe depletion of magne-

sium and the enrichment in aluminium observed in Extreme He enriched stars. In addition taking into consideration the deep mixing in RGB we are also able to reproduce the large spread observed in the Oxygen abundance. This last hypothesis will be easily tested when the measurements of the Oxygen abundance will be available also in main sequence stars of NGC2808 where we expect larger and less dispersed average values than those actually observed in RGB.

## ACKNOWLEDGMENTS

We thank the referee for his/her useful comments and Eugenio Carretta for sharing with us Carretta et al. (2018)'s tables before on-line publication. Flavia Dell'Agli acknowledges support provided by the Spanish Ministry of Economy and Competitiveness (MINECO) under grant AYA-2017-88254-P. Marco Tailo acknowledges support by the European Research Council through the ERC-StG 2016, project 716082 'GALFOR' (<http://progetti.dfa.unipd.it/GALFOR/>) and by the MIUR through the the FARE project R164RM93XW 'SEMPLICE'.

## REFERENCES

- Angulo C., Arnould M., Rayet M., et al. 1999, *Nuclear Physics A*, 656, 3
- Arnould M., Goriely S., Jorissen A. 1999, *A&A*, 347, 572
- Bedin L. R., Piotto G., Anderson J., Cassisi S., King I. R., Momany Y., Carraro G. 2004, *ApJ*, 605, L125
- Blöcker T. 1995, *A&A*, 297, 727
- Blöcker T., Schönberner D. 1991, *A&A*, 244, L43
- Bragaglia, A., Carretta, E., Gratton, R. G., et al. 2010, *ApJ*, 720, L41
- Caloi V., D'Antona F. 2005, *A&A*, 435, 987
- Caloi V., D'Antona F. 2007, *A&A*, 463, 949
- Caloi V., D'Antona F. 2008, *ApJ*, 673, 847
- Canuto V. M., Mazzitelli I. 1991, *ApJ*, 370, 295
- Carretta, E., Bragaglia, A., Gratton, R. G., et al. 2006, *A&A*, 450, 523
- Carretta, E., Bragaglia, A., Gratton, R. G., et al. 2009, *A&A*, 505, 117
- Carretta, E. 2015, *ApJ*, 810, 148
- Carretta E., Bragaglia A., Lucatello S., Gratton R., D'Orazi V., Sollima A. 2018, arXiv:1801.09689
- Cloutman L. D., Eoill J. G. 1976, *ApJ*, 206, 548
- Cohen J. G., Kirby E. N. 2012, *ApJ*, 760, 86
- Cohen J. G., Meléndez J. 2005, *AJ*, 129, 303
- D'Antona F., Caloi V., Montalbán J., Ventura P., Gratton R. 2002, *A&A*, 395, 69
- D'Antona F., Caloi V. 2004, *ApJ*, 611, 871
- D'Antona F., Bellazzini M., Caloi V., Fusi Pecci F., Galletti S., Rood R. T. 2005, *ApJ*, 631, 868
- D'Antona F., Ventura, P. 2007, *MNRAS*, 379, 1431
- D'Antona F., Vesperini E., D'Ercole A., Ventura P., Milone A. P., Marino A. F., Tailo M. 2016, *MNRAS*, 458, 2122 (D16)
- Dell'Agli F., García-Hernández D. A., Ventura P., et al. 2018, *MNRAS*, 475, 3098
- Denisenkov P. A., Denisenkova S. N. 1990, *Soviet Astronomy Letters*, 16, 275
- Denissenkov P. A., Vandenberg D. A., 2003, *ApJ*, 593, 509
- D'Ercole A., Vesperini E., D'Antona F., McMillan S. L. W., Recchi, S. 2008, *MNRAS*, 391, 825
- D'Ercole A., D'Antona F., Ventura P., Vesperini E., McMillan S. L. W. 2010, *MNRAS*, 407, 854
- D'Ercole A., D'Antona F., Vesperini E. 2011, *MNRAS*, 415, 1304
- D'Ercole A., D'Antona F., Vesperini E. 2016, *MNRAS*, 461, 4088
- Di Criscienzo M., D'Antona F., Milone A. P., Ventura P., Caloi V., Carini R., D'Ercole A., Vesperini E., Piotto G. 2011, *MNRAS*, 414, 3381
- Di Criscienzo M., Dell'Agli F., Ventura P., et al. 2013, *MNRAS*, 433, 313
- Di Criscienzo M., Tailo M., Milone A. P., D'Antona F., Ventura P., Dotter A., Brocato E. 2015, *MNRAS*, 446, 1469
- Doherty C. L., Gil-Pons P., Lau H. H. B., Lattanzio J. C., Siess L., Campbell S. W. 2014, *MNRAS*, 441, 582
- Doherty C. L., Gil-Pons P., Siess L., Lattanzio J. C., Lau H. H. B. 2015, *MNRAS*, 446, 2599
- Ferrarotti A. D., Gail H. P., 2006, *A&A*, 553, 576
- Formicola A., Imbriani G., Costantini H., et al. 2004, *Phys. Lett. B*, 591, 61
- Garcia-Berro E., Iben I. 1994, *ApJ*, 434, 306
- García-Berro E., Ritossa C., Iben I. Jr. 1997, *ApJ*, 485, 765
- Gratton R. G., Bonifacio P., Bragaglia A., et al. 2001, *A&A*, 369, 87
- Gratton R. G., Carretta E., Bragaglia A. 2012, *A&AR*, 20, 50
- Hale S. E., Champagne A. E., Iliadis C., et al. 2002, *Phys. Rev. C*, 65, 5801
- Hale S. E., Champagne A. E., Iliadis C., et al. 2004, *Phys. Rev. C*, 70, 5802
- Iben I., Ritossa C., Garcia-Berro E. 1997, *ApJ*, 489, 772
- Kraft, R. P., Sneden, C., Smith, G. H., et al. 1997, *AJ*, 113, 279
- Mészáros S., Martell S. L., Shetrone M., et al. 2015, *AJ*, 149, 153
- Milone A. P. et al., 2015, *ApJ*, 808, 51
- Mowlavi N. 1999, *A&A*, 350, 73
- Mucciarelli A., Bellazzini M., Ibata R., Merle T., Chapman S. C., Dalessandro E., Sollima A. 2012, *ApJ*, 426, 2889
- Piotto G., Bedin L. R., Anderson J., et al. 2007, *ApJL*, 661, L53
- Piotto G., Milone A. P., Bedin L. R., et al. 2015, *AJ*, 149, 91
- Renzini A., Voli M., 1981, *A&A*, 94, 175
- Ritossa C., Garcia-Berro E., Iben I. Jr. 1996, *ApJ*, 460, 489
- Siess L. 2006, *A&A*, 448, 717
- Siess L. 2007, *A&A*, 476, 893
- Siess L., Arnould, M. 2008, *A&A*, 489, 395
- Siess L. 2010, *A&A*, 512, A10
- Sneden, C., Kraft, R. P., Guhathakurta, P., Peterson, R. C., & Fulbright, J. P. 2004, *AJ*, 127, 2162
- Tailo M., D'Antona F., Vesperini E., et al. 2015, *Nature*, 523, 318
- Tailo M., Di Criscienzo M., D'Antona, F., Caloi V., Ventura P. 2016, *MNRAS*, 457, 4525
- Ventura P., Zeppieri A., Mazzitelli I., D'Antona F., 1998,

- A&A, 334, 953  
Ventura P., D'Antona F., Mazzitelli, I. 2000, A&A, 363, 605  
Ventura P., D'Antona F., Mazzitelli I., Gratton, R. 2001, ApJL, 550, L65  
Ventura P., D'Antona F. 2006, A&A, 457, 995  
Ventura P., D'Antona F. 2008, MNRAS, 385, 2034  
Ventura P., & D'Antona F. 2009, A&A, 499, 835  
Ventura P. 2010, Light Elements in the Universe, 268, 147  
Ventura, P., & D'Antona, F. 2011, MNRAS, 410, 2760  
Ventura P., D'Antona F., Di Criscienzo M., Carini R., D'Ercole A., Vesperini E. 2012, ApJL, 761, L30  
Ventura P., Di Criscienzo M., Carini R., D'Antona F., 2013, MNRAS, 431, 3642  
Ventura P., Dell'Agli F., Schneider R., et al. 2014, MNRAS, 439, 977  
Ventura P., García-Hernández D. A., Dell'Agli F., et al. 2016, ApJL, 831, L17  
Ventura, P., D'Antona, F., Imbriani, G., et al. 2018, MNRAS, 477, 438  
Vesperini E., McMillan S. L. W., D'Antona, F., D'Ercole, A. 2013, MNRAS, 429, 1913